Pergamon

Bioorganic & Medicinal Chemistry, Vol. 5, No. 6, pp 1197–1207, 1997

PII: S0968-0896(97)00062-X
0968-0896/97 $17.00 + 0.00

Selectivity of F8-Actinomycin D for RNA:DNA Hybrids and its Anti-Leukemia Activity

Fusao Takusagawa, Ken T. Takusagawa, Robert G. Carlson and Robert F. Weaver
Department of Biochemistry, University of Kansas, Lawrence, KS 66045-2106, U.S.A.

Abstract—Although many compounds have been found that bind to DNA in various ways and exhibit various biological activities, few compounds that specifically bind to RNA or RNA:DNA hybrids are known, even though such compounds are expected to have important biological properties. For example, one characteristic function of the retroviruses, which is generally not found in eukaryotic cells, is the production of an RNA:DNA hybrid in the viral replication phase. If an agent is designed to bind only to an RNA:DNA hybrid, and not to DNA or to RNA, such an agent might be able to inhibit specifically the RNase H activity of retroviral reverse transcriptase, and therefore suppress viral replication. Actinomycin D is known to bind to double-stranded DNA, but not to RNA, because steric hindrance between the 2-amino group of the phenoxazone ring and the 2′-hydroxyl group of RNA prevents intercalation of the compound. However, if the >C-H moiety at the 8-position of the phenoxazone ring is replaced by a >C-F, a possible hydrogen-bond acceptor, this analogue (8-fluoro-actinomycin D, F8AMD) might be able to bind intercalatively to an RNA:DNA hybrid by forming an additional hydrogen bond between F8 and the 2′-hydroxyl group of the guanosine ribose. To test this hypothesis, the crystal structure of d(GAAGCTTC)$_2$-F8AMD has been determined at 3.0 Å resolution. Based on this crystal structure, a model in which F8AMD binds into the hybrid r(GAAGCUUC):d(GAAGCTTC) has been built using molecular mechanics and dynamic methods. These structural studies indicate that F8AMD binds intercalatively to a B-form double-stranded DNA whereas the drug intercalates into an RNA:DNA hybrid taking an A-form conformation. In the RNA:DNA hybrid complex, the F8 atom is located so as to be able to interact to an O2′ hydroxyl group with either an O-H···F hydrogen bond or $H^+ \cdots F^-$ electrostatic interaction. This interaction might stabilize the F8AMD molecule in the RNA:DNA hybrid. A binding study indicates that both actinomycin D (AMD) and F8AMD bind intercalatively not only to double-stranded DNAs, but also to RNA:DNA hybrids. Although the overall binding capacity of F8AMD ($k = 4.5 \times 10^5\ M^{-1}$) is reduced slightly in comparison with AMD itself ($k = 1.8 \times 10^6\ M^{-1}$), F8AMD tends to bind relatively more favorably than AMD to the RNA:DNA hybrids. The drugs' effects on RNA synthesis in HeLa cells indicates that the binding capacities of AMD and F8AMD correlates strongly to their RNA synthesis inhibitory activities. F8AMD required a concentration of 78 nM to inhibit RNA polymerase activity in HeLa cells by 50%, whereas AMD reached the same inhibitory level at 30 nM. Surprisingly, F8AMD exhibits unique selectivity against leukemia cells as does another C8-derivatized AMD analogue, N8AMD. F8AMD inhibits 50% of leukemia cell growth at less than 1.0 nM whereas 10- to 130-fold-higher drug concentrations are required to inhibit the growth of other tumor cell lines by 50%. The GI_{50} value of F8AMD for leukemia cells is the lowest among the GI_{50} values for all other AMD derivatives tested. By contrast, AMD is quite potent and kills most cells at less than 50 nM concentration, but it does not show any selectivity for certain cell lines. This indicates that AMD should have very limited use as an antitumor agent. It is difficult to rationalize why F8AMD and N8AMD show such strong selectivity against leukemia cells. However, this study and our previous study (*J. Am. Chem. Soc.* **1994**, *116*, 7971) indicated that F8AMD and N8AMD tended to bind more favorably to RNA:DNA hybrids. Thus, the unique antileukemia selectivity shown by F8AMD and N8AMD might be caused by the agents binding to RNA:DNA hybrids rather than to double-stranded DNA. © 1997 Elsevier Science Ltd.

Introduction

A large number of compounds are known that bind to DNA in various ways. A subset of those bind in the minor groove via a noncovalent interaction, intercalate between base pairs, and form a covalent bond with DNA.[1] The physical and biological characteristics of these compounds have been studied, since some of them act as anticancer agents and others as carcinogens. On the other hand, few compounds are known that bind in the same fashion, but specifically to RNA or RNA:DNA hybrids.

RNA or RNA:DNA hybrid binding compounds might carry important biological properties. For example, HIV reverse transcriptase uses a lysine transfer RNA as a primer to make a minus strand DNA copy of the viral RNA as an RNA:DNA hybrid.[2] Beside having reverse transcriptase activity, the enzyme possesses an inherent RNase H activity that specifically degrades the RNA of the RNA:DNA hybrid.[3–8] Therefore, in theory, inhibition of this process would suppress viral replication. Thus, we are looking for agents that bind only to an RNA:DNA hybrid, and not to double-stranded DNA or to RNA. Such agents might specifically inhibit the RNase H activity of reverse transcriptase and, therefore, suppress viral replication.

Biological studies have indicated that actinomycin D (AMD), shown in Figure 1, moderately inhibits reverse transcriptase activity.[9,10] In vitro, a 50% inhibition of reverse transcriptase activity is reached at a 35 μg/mL (28 μM) concentration of AMD, and a 50% inhibition of RNA polymerase activity is reached at a 1.5 μg/mL (1.2 μM) concentration of AMD.[9] The experimental

data obtained from the inhibition of reverse transcriptase activity by ribonuclease and AMD suggest that the antibiotic does not inhibit the synthesis of the RNA:DNA hybrid from viral RNA, but does inhibit the subsequent synthesis of double-stranded DNA, and the inhibited reaction produces low molecular weight double-stranded DNA.[10] These experimental results suggest that AMD might bind intercalatively to the RNA:DNA hybrid, and the intercalated agent inhibits the RNase H activity of retroviral reverse transcriptase.

Recently, we have determined the crystal structures of several complexes between d(GAAGCTTC)$_2$ and AMD crystallized in the space groups *C*2[11] and *F*222[12] and complexed with N^8-actinomycin D (N8AMD)[13] in which AMD and N8AMD intercalated between the middle 5′-GC-3′ base pairs. These crystal structures of the complexes show how the drug interacts with DNA, and may explain why AMD cannot bind to RNA. The 2′-hydroxyl group of ribose would be in unusually close proximity to the 2-amino group of the phenoxazone ring, if the deoxyribose of the guanosine were changed to ribose. The interaction between these two groups would make it impossible for AMD to bind to RNA. However, if the C-H moiety at the 8-position of the phenoxazone ring is replaced by the strong hydrogen-bond acceptor nitrogen atom (N8), the 2′-hydroxyl group of the guanosine ribose (RNA) will be able to make a hydrogen bond to N8. To test our hypothesis, we have synthesized N8AMD and examined the binding character of the agent to nucleic acids.[14] This study indicated that N8AMD binds intercalatively not only to double-stranded DNA but also to RNA:DNA hybrids. However, the binding capacity of N8AMD to both double-stranded DNA and to RNA:DNA hybrids was drastically reduced, probably due to the hydration of the N8, which prevented the drug from intercalating into the nucleic acids. This hydration also reduced the drug's diffusion into the cells. Consequently, the biological activity of N8AMD was substantially reduced. Thus, it is important to design compounds that interact selectively with RNA:DNA hybrids such that neither binding capacity nor lipophilicity is lost.

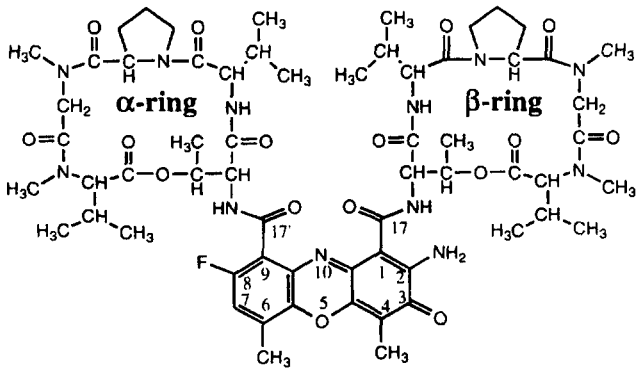

Figure 1. Molecular formula of 8-fluoro-actinomycin D (F8AMD). The hydrogen at the 8-position of the phenoxazone ring of actinomycin D (AMD) was replaced with a fluorine atom. For the N8-actinomycin D (N8AMD), the C-H moiety at the 8-position of the phenoxazone ring was replaced with a nitrogen atom.

As the second smallest substituent, fluorine most closely mimics hydrogen with respect to steric requirements at RNA:DNA hybrid binding sites. Furthermore, the high electronegativity of fluorine frequently alters electronic effects and, therefore, the fluorine can act as a hydrogen acceptor. The presence of fluorine often leads to increase lipid solubility, thereby enhancing rates of absorption and transport of drugs in vivo.[15] Therefore, we have modified the 8-position of the phenoxazone ring by replacing the >C-H with >C-F. Here we report on the structures of d(GAAGCTTC)$_2$–F8AMD and r(GAAGCUUC):d(GAAGCTTC)–F8AMD complexes, and the binding characteristics and biological activities of F8AMD in comparison with AMD.

Results and Discussion

Structures of F8AMD complexes

Since the crystal structure of the d(GAAGCTTC)$_2$–F8AMD complex is an isomorphous structure of d(GAAGCTTC)$_2$–N8AMD,[13] the structure will be briefly detailed here (Table 1). The structure of the r(GAAGCUUC):d(GAAGCTTC)–F8AMD complex was built based on the crystal structure of the DNA:DNA–F8AMD complex since we have not grown crystals of RNA:DNA hybrids complexed with F8AMD. The RNA:DNA hybrid complex structure has been refined to minimize the total energy in the same crystal system of the DNA:DNA–F8AMD complex using the X-PLOR. It is noted that the structures of d(GAAGCTTC)$_2$–F8AMD and r(GAAGCUUC):d(GAAGCTTC)–F8AMD complexes are determined by different methods. Thus these structures cannot be compared directly in detail. However, the DNA:DNA–F8AMD crystal structure refined by a similar molecular modeling procedure was convergent to a structure similar to the original crystal structure, indicating that the molecular modeling method using the X-PLOR software can produce results similar to those obtained from the X-ray crystal structure analysis in this case. Thus, the molecular modeling structure of the F8AMD molecule complexed with the r(GAAGCUUC):d(GAAGCTTC) hybrid can be considered to have a

Table 1. The RMS deviations (Å) of the DNA:DNA–N8AMD crystal structure and the RNA:DNA–F8AMD model structure from the crystal structure of DNA:DNA–F8AMD

Portion	DNA:DNA–N8AMD	RNA:DNA–F8AMD
Complex	0.83	2.39
DNA:DNA or RNA:DNA	0.78	2.38
Strand-1 (N2-amino group side)	0.89	2.00
Strand-2 (N8-atom side)	0.58	2.18
Drug	0.79	1.14
Phenoxazone ring	0.08	0.03
Depsipeptide ring (α-ring)	0.21	1.34
Depsipeptide ring (β-ring)	0.69	1.20

similar quality to that of the crystal structure. For this reason, we will compare the DNA:DNA and RNA:DNA complex structures in order to elucidate some physical and biological characteristics of F8AMD.

As schematically illustrated in Figure 2, the chromophore of the F8AMD molecule intercalates via the minor groove into the middle (5′-GC-3′) of the oligonucleotide, and the two cyclic depsipeptides lie on both sides of the minor groove. The DNA numbering and standard convention are illustrated in Figure 2. The DNA:DNA and RNA:DNA hybrid helices are unwound by about 30 at the intercalation site, G4–C5, and the G4≡C13 and C5≡C12 base pairs are stretched to ≈7.0 Å (Table 2). The two cyclic depsipeptide rings cover four base-pairs (A3=T14, G4≡C13, C5≡G12, and T6=A11) of the DNA (Fig. 3). F8AMD is tightly connected to the DNA:DNA double-strand and RNA:DNA hybrid at the middle portion of the molecule by forming four threonine–guanine hydrogen bonds and an additional hydrogen bond between the N2 amino group of phenoxazone and the DNA backbone. The four threonine–guanine hydrogen bonds appear to recognize the DNA sequence 5′-GC-3′ as pointed out by Sobell and Jain.[16] These essential hydrogen bonds are covered by cyclic depsipeptides, which are constructed with mainly hydrophobic amino acid residues. These binding features of F8AMD are the same as those found in the AMD complexes[11,12] and N8AMD complex.[13] The complexes are stacked together to form a pseudo-continuous helix running through the crystals. Stereoscopic views of the pseudo-continuous helices of the crystal structure and the molecular modeling structure are illustrated in Figures 3 and 4.

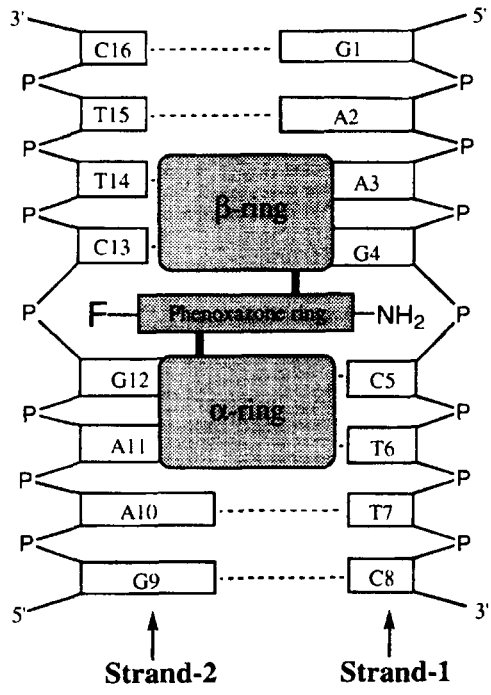

Figure 2. Schematic diagram of the d(GAAGCTTC)$_2$-F8AMD as observed in the crystal structure. The DNA strand numbered G1-A2-A3-G4-C5-T6-T7-C8, which is located on the side of the amino group (NH_2) of the chromophore, is named strand-1; the other DNA strand numbered G9-A10-A11-G12-C13-T14-T15-C16, which is located on the side of the F8 atom, is named strand-2. The cyclic depsipeptide attached at C9 of the chromophore is called the α-ring, and the other cyclic depsipeptide, which is attached at C1 and is near the amino group (NH_2), is called the β-ring.[17]

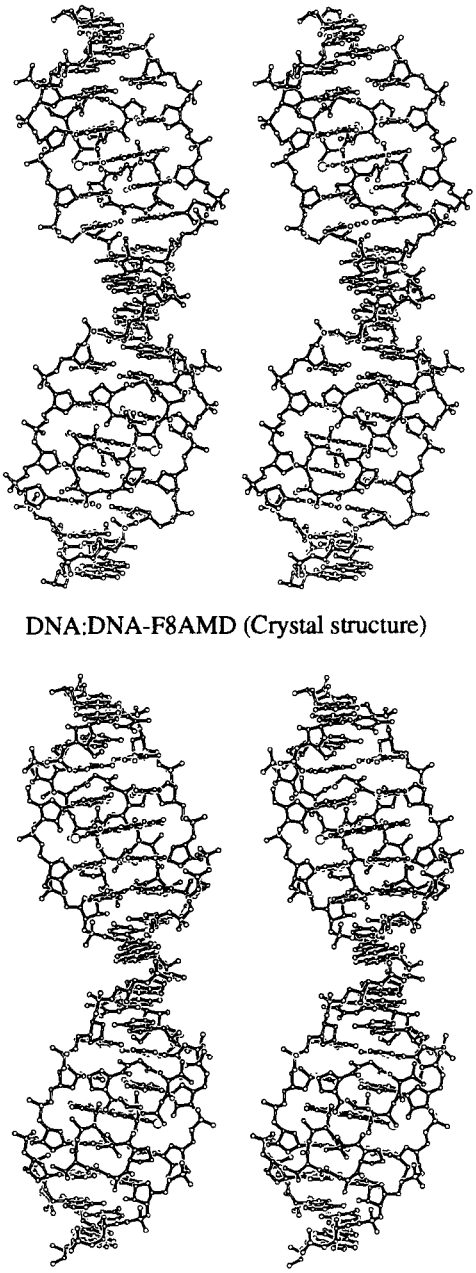

Figure 3. Stereo drawings of the pseudo-continuous helical structures of the d(GAAGCTTC)$_2$–F8AMD complex (A), and a model structure of r(GAAGCUUC):d(GAAGCTTC)–F8AMD complex (B). The top and bottom portions of the helix represent the views of the major and minor grooves, respectively. The α-ring and β-ring of the cyclic depsipeptides are below and above the phenoxazone ring, respectively. The F8AMD and RNA strand are illustrated with solid bonds while the DNA strands have open bonds. The F8 atoms in the F8AMD molecules are indicated by large open circles.

Table 2. Helix twist angles and base-pair rise parameters[a]

	Helix twist angles (°)							
	G1–A2	A2–A3	A3–G4	G4–C5	C5–T6	T6–T7	T7–C8	Mean
Crystal structure	40	47	29	9	19	33	32	30
RNA:DNA model	35	39	31	16	27	32	25	29
	Base-pair rise (Å)							
	G1–A2	A2–A3	A3–G4	G4–C5	C5–T6	T6–T7	T7–C8	Mean[b]
Crystal structure	2.7	4.0	3.0	6.8	4.1	2.7	3.2	3.3
RNA:DNA model	1.5	2.4	2.3	6.5	3.2	3.4	1.4	2.4

[a]The helix twist angles and base-pair rise parameters are defined and calculated by the procedures recommended at the EMBO Workshop on DNA Curvature and Binding held at Churchill College in 1988.
[b]The mean values calculated by excluding the rise at the intercalation site (G4–C5).

In the DNA:DNA–F8AMD complex structure, the substituted F8 atom does not participate in any hydrogen bonds to DNA (Fig. 5A) although the C2′-H might be involved in a weak C-H···F hydrogen bond with F8. The backbone of the DNA strand-2, which is located on the same side as the F8 atom, lies far away from the F8 atom. In particular, the phosphate group between the G12 and C13 residues is located as if the negatively charged PO_4 group is pushed far away by the negatively charged F8 atom, whereas the backbone of the other DNA strand (strand-1) is significantly bent at the intercalation site (Fig. 4) because of hydrogen bonds between the amino group (N2) attached to the phenoxazone ring and oxygen atoms of backbone (Fig. 5).

In the RNA:DNA hybrid complex, the F8 atom is located so as to be able to interact with the O2′ hydroxyl group with either a O-H···F hydrogen bond or $H^+\cdots F^-$ electrostatic interaction (Fig. 5B). This interaction might stabilize the F8AMD molecule in the RNA:DNA hybrid. Unlike the double-stranded DNA, both DNA and RNA strands in the RNA:DNA hybrid are bent slightly at the intercalation sites, and there is no significant overall conformational difference between the two strands. Since the intercalation of F8AMD very much distorts the structures of double-stranded DNA and RNA:DNA hybrid, it is difficult to imagine the initial structures of the nucleotides. However, when the structures of the DNA:DNA and RNA:DNA hybrid complexes are compared to each other, we can see a significant difference between these structures (Fig. 4 and Table 1). The RNA:DNA hybrid has a wide and very deep major groove, exhibiting a typical A-form conformation. This observation is consistent with the crystal structures of RNA:DNA hybrids.[18,19] In light of the RNA:DNA hybrid complex structure, the DNA:DNA structure is apparently a kinked B-form structure. The helical parameters analyzed with the HELIB software[20] listed in Table 2 support the above conclusion. For example, the mean base-pair rises of DNA:DNA and RNA:DNA are 3.3 and 2.4 Å, respectively. Therefore, these crystallographic and molecular modeling studies indicate that the F8AMD molecule binds intercalatively into different forms of nucleic acids, that is, a B-form DNA:DNA and an A-form RNA:DNA hybrid.

Binding study

From the crystal structures of DNA:DNA–AMD,[11,12] DNA:DNA–N8AMD,[13] and DNA:DNA–F8AMD complexes, it is very clear that the chromophore of AMD cannot bind to the major/minor groove of DNA as do typical minor groove binding agents, such as netropsin and distamycin,[21] since there are not enough polar groups (-NH, -OH, >N, =O and >O) on the surface of the chromophore. Therefore, the binding modes available to AMD and F8AMD are either intercalation or weak side-binding to the charged phosphate backbone of DNA. Since the visible spectrum (350–600 nm) of the chromophore is slightly shifted to the longer wavelength region (red shift) and the magnitude of absorbance is reduced (hypochromic effect) by the drug intercalating into the nucleic acid, the binding characteristics of AMD and F8AMD can be observed in the spectra by titration with DNA solutions.

In the previous N8AMD study,[14] two nonself complementary G/C-rich sequences, 5′-GGAGCAGGAC-3′ and 5′-G(T/U)CC(T/U)GC(T/U)CC-3′, were utilized to measure the association constants. There were two major problems in the experiment. One was the uncertain ratio of the two strands and the other was the interpretation of the visible spectra since the G/C-rich sequences have possible multiple binding sites for AMD and N8AMD. Therefore, in this study, two hairpin stem-loop sequences (Fig. 6) have been selected for examination of the binding characteristics of F8AMD based on the following considerations. (1) The hairpin stems have only one drug-binding sequence GC in the middle. Thus, the visible spectra of AMD and F8AMD titrated by the hairpin stem-loops can be interpreted relatively simply. (2) Unlike two separated nonself-complementary sequence strands, the hairpin stem-loops can form an exact 1:1 ratio duplex in the stem region. (3) Nonself-complementary sequences are selected in the stem section in order to prevent dimerization of two hairpin stem-loops. (4) Purine–pyrimidine alternating sequences are selected in the

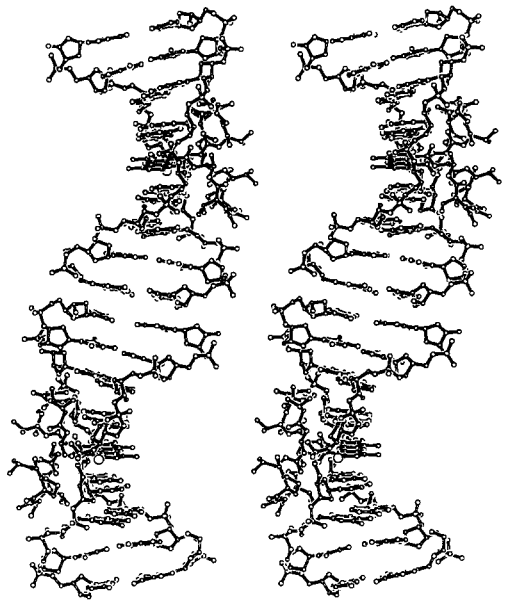

DNA:DNA-F8AMD (Crystal structure)

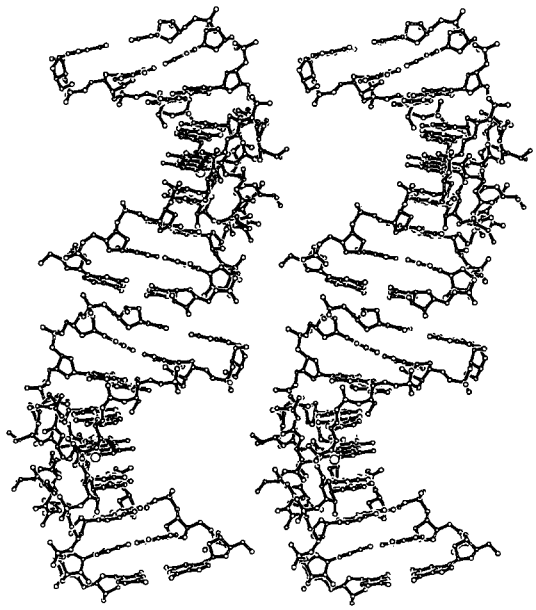

RNA:DNA-F8AMD complex (Molecular modeling structure)

Figure 4. Stereo drawings of the pseudo-continuous helical structures of the d(GAAGCTTC)$_2$–F8AMD complex (A) and a model structure of the r(GAAGCUUC):d(GAAGCTTC)–F8AMD complex (B). The top and bottom portions of the helix represent the DNA strand-1 and strand-2 on the same side as the amino group (N2) and the F8 atom of the phenoxazone ring, respectively. The α-ring and β-ring of the cyclic depsipeptides are below and above the phenoxazone ring, respectively. The F8AMD and RNA strand are illustrated with solid bonds, while the DNA strands have open bonds. The F8 atoms in the F8AMD complex are indicated by large open circles.

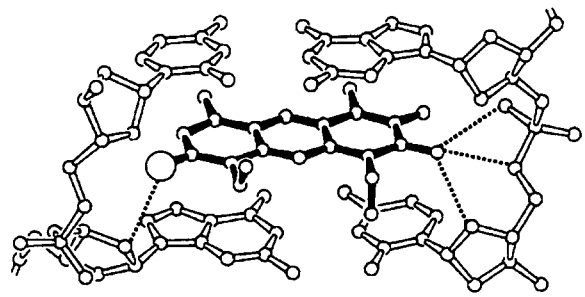

DNA:DNA-F8AMD complex (Crystal structure)

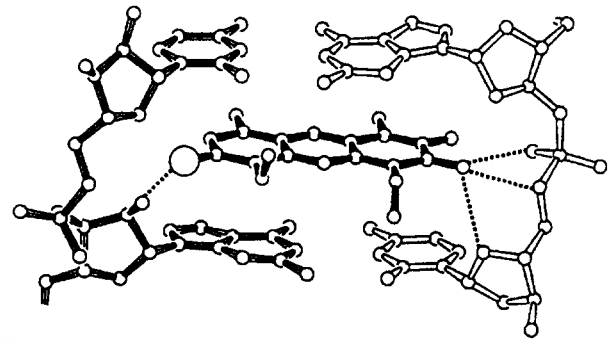

RNA:DNA-F8AMD complex (Molecular modeling structure)

Figure 5. Environment surrounding the F8 atom. (A) Crystal structure of the d(GAAGCTTC)$_2$–F8AMD complex. (B) Molecular modeling structure of the r(GAAGCUUC):d(GAAGCTTC)–F8AMD complex. Possible polar interactions involving F8 and the N2 amino group are indicated by dotted lines. The phenoxazone ring of F8AMD, DNA strands (G4–C5 and G12–C13) and RNA strand (G12–C13) are illustrated by solid bonds, open bonds, and shaded bonds, respectively. The F8 atoms are drawn with larger circles.

stem region since the alternating sequences form a stable double-stranded helix even at a relatively low concentration (≈ 0.2 μM). Melting experiments indicate that the DNA:DNA and RNA:DNA hairpin stem-loops indeed form double helices under 7 °C.

The visible absorption spectra of F8AMD and AMD were measured at seven different concentrations of the oligonucleotides (Fig. 7). The spectra generated by titration with the DNA:DNA and RNA:DNA hairpin stem-loops show significant red shifts as well as hypochromic effects, indicating that the F8AMD and AMD bind intercalatively to -GC- sites of the hairpin-stems. These spectra show clearly that both AMD and F8AMD bind intercalatively not only to the DNA:DNA double-strands, but also bind to the RNA:DNA hybrids. Since AMD does bind to the RNA:DNA hybrid, this result supports the earlier observation,[10] in which AMD inhibited the reverse transcriptase activity in synthesis of double-stranded DNA from an RNA:DNA hybrid, but did not inhibit the synthesis of an RNA:DNA hybrid from a single RNA strand. It should be noted that several old experimental data,[22] which suggested that AMD does not bind to an RNA:DNA hybrid, appear to have been misinterpreted. Moreover the binding capacity of AMD to the RNA:DNA hybrid is significantly reduced, indicating that the drug has much higher affinity for the B-form nucleic acids than for the A-form nucleic acids.

The spectra were analyzed quantitatively by a method described in our previous paper[23] (Table 3). The binding constants for AMD and F8AMD with the hairpin stem-loops indicate that AMD molecules bind more strongly to both oligonucleotides than do the

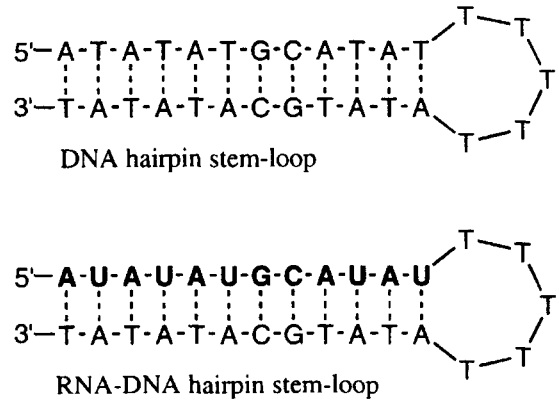

Figure 6. DNA–DNA and RNA–DNA hybrid hairpin stem-loops. The AMD and F8AMD binding sites (5′-GC-3′) are located at the middle of the stem. The RNA region is illustrated with bold letters.

F8AMD molecule. Dixon and Smart have demonstrated that the fluorine atoms in enols and alcohols form intramolecular HF hydrogen bonds.[24] Thus, the F8AMD molecule might form an additional hydrogen bond with a water molecule (F8···H-O-H) in aqueous solution, which cannot form with the AMD molecule. This hydrogen bonding would stabilize the F8AMD molecules in solution and tend to prevent intercalation of the F8AMD molecules into the nucleic acid. As a result, the binding constant of F8AMD ($k = 4.5 \times 10^5$ M^{-1}) is less than that of AMD ($k = 1.8 \times 10^6$ M^{-1}). However, this trend is much smaller than that observed in the N8AMD case, in which the association constant was reduced by nearly 100-fold[14] because the aromatic nitrogen is more strongly hydrated in aqueous solution. The other significant difference between AMD and F8AMD is the ratio of binding constants with DNA:DNA and RNA:DNA. The ratio of DNA:DNA–AMD and RNA:DNA–AMD is 7 ($1.8 \times 10^6 \div 2.6 \times 10^5 = 7$), whereas the corresponding ratio of DNA:DNA–F8AMD and RNA:DNA–F8AMD is 3 ($4.5 \times 10^5 \div 1.4 \times 10^5 = 3$). This difference between the ratios indicates that the F8AMD molecule binds relatively more favorably to the RNA:DNA hybrid than the AMD molecule. Such a tendency toward RNA:DNA hybrid selectivity of F8AMD was expected because of the introduction of the F8-atom into the chromophore. The

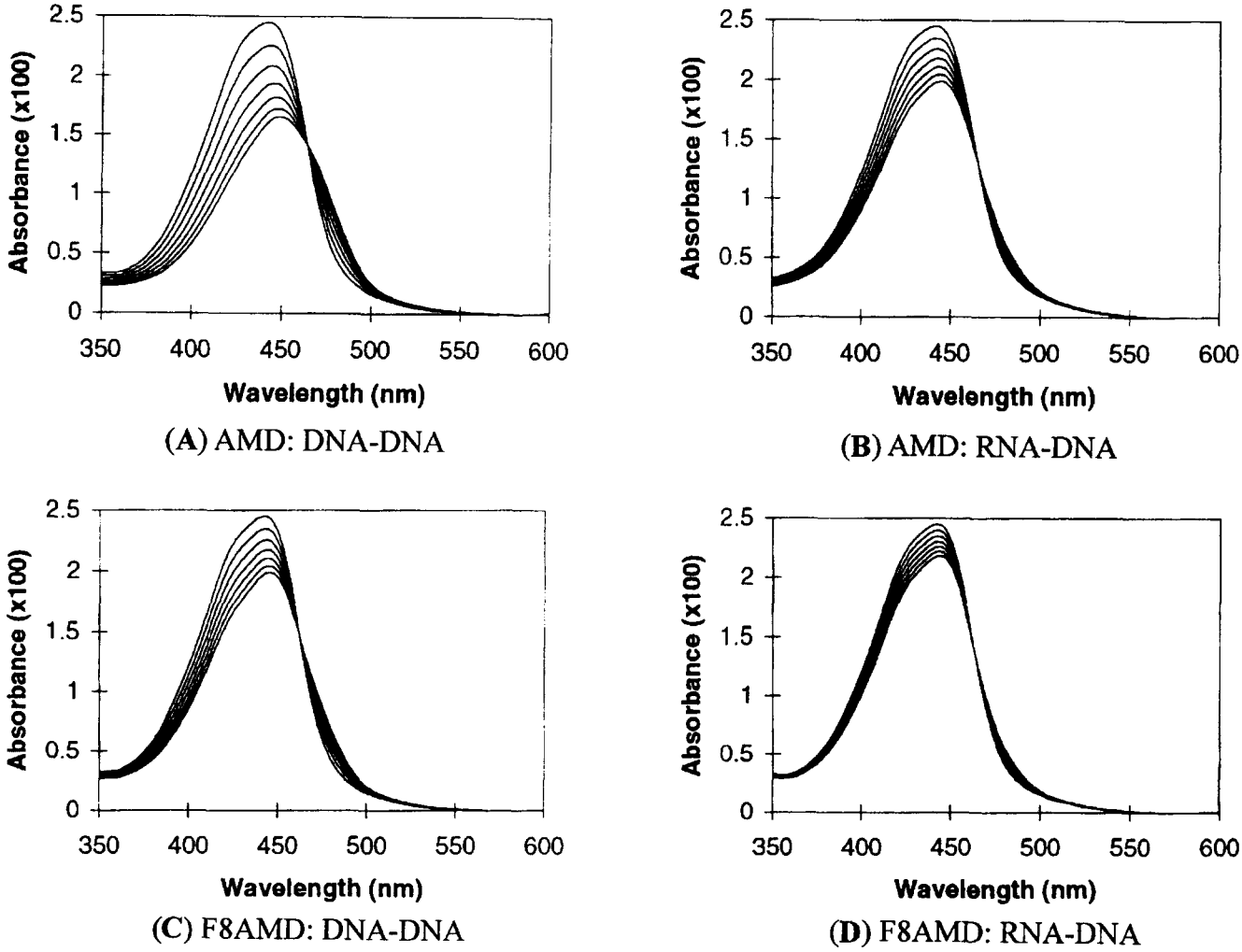

Figure 7. Visible absorption spectra of AMD and F8AMD titrated with the DNA–DNA and RNA–DNA hybrid hairpin stem-loops illustrated in Figure 6. (A) AMD titrated with DNA–DNA hairpin stem-loop, (B) AMD titrated with RNA–DNA hairpin stem-loop, (C) F8AMD titrated with DNA hairpin stem-loop, and (D) F8AMD titrated with RNA–DNA hairpin stem-loop. The drug concentration is scaled to 1.0 μM. The ratios of [DNA]/[drug] of 0.0, 0.2, 0.4, 0.6, 0.8, 1.0, 1.2 progress from the highest curve downward.

Table 3. Association constant (k M^{-1}), hypochromic effect (H) and red shift ($\Delta\lambda$ nm) of AMD and F8AMD with DNA hairpin stem-loop (DNA:DNA) and RNA:DNA hairpin stem-loop (RNA:DNA)

	AMD			F8AMD		
	$k \times 10^5$	H	$\Delta\lambda$	$k \times 10^5$	H	$\Delta\lambda$
DNA:DNA	18.0	0.58	21	4.5	0.60	22
RNA:DNA	2.6	0.52	22	1.4	0.56	24

F8-atom probably participates in an additional hydrogen bond (F8···H-O2′) with the 2′-hydroxyl group of RNA in the RNA:DNA–F8AMD complex. Although such a hydrogen bond cannot be formed in the RNA:DNA–AMD complex, the crystal structure of the DNA:DNA–F8AMD complex indicates the presence of a weak C2′-H···F8 hydrogen bond.

RNA polymerase inhibitory activity of F8AMD

The RNA polymerase inhibitory activities of F8AMD, N8AMD, and AMD in vivo have been examined using human cells (HeLa). The drug concentrations at 50% inhibition level (IC_{50}) are listed in Table 4 along with the mean 50% growth inhibition (GI_{50}) of various tumor cell lines. The DNA association constants and the IC_{50} values correlate well, indicating that the tighter an agent binds to DNA:DNA, the better it inhibits transcription activity. Although the DNA binding mode of F8AMD is quite similar to that of AMD in the crystal, the RNA synthesis inhibitory activity is reduced by half. A similar trend is clearly observed in the anticancer activity data, as will be discussed below.

Anticancer activity of F8AMD

The anticancer activities of AMD, F8AMD, and N8AMD were examined using 60 different human tumor cell lines in culture at the National Cancer Institute of the National Institutes of Health (Table 4).

Table 4. Drug concentration (GI_{50}, nM) at 50% growth inhibition of various tumor cell lines carried out at the NCI, and RNA synthesis inhibitory activities (IC_{50}, nM) in HeLa cells

Tumor cell lines	AMD (nM)	F8AMD (nM)	N8AMD (nM)
Leukemia	**2.29**	**<1.00**	**214**
Lung	1.17	28.8	3160
Colon	1.20	14.1	2820
CNS	1.12	12.3	1350
Melanoma	1.23	11.5	1540
Ovarian	1.95	102	5248
Renal	2.69	129	5370
Prostate	1.66	44.7	4570
Breast	2.14	55.0	5250
Mean	1.62	23.4	24.50
IC_{50}[a]	34.6	77.6	>5000

[a]Drug concentration at 50% inhibition of RNA synthesis in HeLa cells.

The mean graphs of the total growth inhibition (TGI) by AMD, F8AMD, and N8AMD are illustrated in Figure 8. The mean concentration of total growth inhibition by F8AMD is 1900 nM, which is much higher than the 48 nM value of AMD, indicating that F8AMD is less potent. This trend is quite consistent with the weaker association constant of F8AMD and its weaker inhibition of transcription in vivo. However, it should be noted that F8AMD exhibits excellent selectivity against leukemia cell lines (Fig. 8 and Table 4). F8AMD inhibits 50% of the leukemia cell growth at less than 1.0 nM whereas 10- to 130-fold-higher drug concentrations are required to inhibit by 50% the growth of the rest of the tumor cell lines. It should be noted that the GI_{50} value of F8AMD for leukemia is lower than any of the AMD IG_{50} values. Although the potency of N8AMD is much lower than AMD and F8AMD, N8AMD exhibits a similar antileukemia selectivity (Fig. 8 and Table 4). It is difficult to explain why F8AMD and N8AMD have such strong selectivity against leukemia cells. However, this study and our previous study[14] indicated that F8AMD and N8AMD tended to bind more favorably to RNA:DNA hybrids. Thus, the unique antileukemia selectivity exhibited by F8AMD and N8AMD might be caused by the agents binding to RNA:DNA hybrids rather than to DNA:DNA. By contrast, AMD is quite potent and kills most cells at less than 50 nM concentration, but it does not show any selectivity for certain cell lines. This indicates that AMD should have very limited use as an antitumor agent.

Experimental

Crystallization of the F8AMD complex

Several self-complementary octa-nucleotides, d(ZYXGCX′Y′Z′), which contain the AMD binding sequence, 5′-XGCX′-3′ (X ≠ G and X′ ≠ C),[25] in the middle, were synthesized by using a fully automated DNA synthesizer (Cruachem P250). The residues X and Y in the sites adjacent to the intercalation site were A or T, and the edge residue Z was C or G to prevent opening of the double helix. Reverse phase HPLC was used to obtain pure oligonucleotides. F8AMD was synthesized totally in our laboratory with a method analogous to that of N8AMD.[14] Relatively large complex crystals were grown under the same conditions as d(GAAGCTTC)$_2$–N8AMD.[13] A typical crystallization mixture contained 2.0 mM oligonucleotide, 10 mM $MgCl_2$, 20 mM cacodylate/HCl (pH 7.0), 2 mM spermine tetrachloride, and 1.5 mM F8AMD in 7.5% (v/v) 2-methyl-2,4-pentanediol (MPD). Hanging drops (20 μL) of the mixture were equilibrated with 15% MPD in an incubator at 26 °C by vapor diffusion. Orange–red crystals appeared after one month.

Structure determination of the F8AMD complex

A hexagonal plate-shaped crystal (0.3 × 0.3 × 0.1 mm) of the DNA–F8AMD complex was mounted into a glass

capillary with mother liquor. The data were measured on a locally modified DIP100S imaging plate X-ray diffractometer (MAC Science) at room temperature using graphite-monochromated CuKα radiation (λ = 1.5418). The still photographs indicated that the crystal diffracted to 3.0 Å resolution. The unit cell dimensions were determined from the still photographs by software developed locally, and were further refined, along with the crystal orientation, by the ELMS software associated with DIP100S.[26] The unit cell dimension and the crystal system (trigonal) indicate that the crystal structure of the DNA–F8AMD complex is an isomorphous structure of that of the DNA–N8AMD complex. The diffraction data were measured up to 3.0 Å resolution. Integrated intensities of the reflections were scaled and reduced with locally developed programs.[27] A total of 1839 independent reflections in 7–3 Å resolution were obtained and were used in subsequent structure determination and refinement.

The initial model was built from the DNA–N8AMD complex structure by replacing the >N with the >C-F moiety at the 8-position of the phenoxazone ring. This model gave an R value of 0.38 for the 7–3 Å resolution data, indicating that the DNA–F8AMD complex structure is indeed isomorphous to that of the DNA–N8AMD complex. The structure was further refined using the method of simulated annealing with the program X-PLOR.[28] The progress of refinement was followed by inspection of electron density maps on a graphics workstation using FRODO.[29] Since the bases formed Watson–Crick base-pairs, those base-pair hydrogen bonds were constrained in the refinement. Refinement of the isotropic temperature factor for individual atoms was carried out by the individual B-factor refinement procedure of X-PLOR using bond and angle restraints. The anisotropic zone scaling procedure was applied in order to correct the absorption effect and/or unknown systematic error in the observed structure factors. No water molecules were introduced in the refinement. The crystallographic data are listed in Table 5. The atomic coordinates have been deposited with the Nucleic Acid Database (entry name: DDH071).

Precise conformational details, accurate hydrogen-bond geometry, contact distances, and features such as the positions of water molecules—all of which may be significant for complete understanding of DNA/RNA–drug interaction—will be visible only at higher resolution. The structure determined at around 3.0 Å resolution, however, provides relatively accurate positions and orientations of rigid groups, such as bases and base pairs. The overall conformations of the DNA backbone and cyclic peptide rings are also visible at this resolution. Intermolecular interactions, mainly hydrogen bonds, are distinguishable. Thus, we believe our present structure to be sufficiently well determined to address many key questions regarding DNA–F8AMD interactions.

Table 5. Crystallographic and refinement data

Molecular form	d(GAAGCTTC)$_2$–F8AMD ($C_{78}H_{92}N_{30}P_7O_{46})_2$–$C_{62}FH_{85}N_{12}O_{16}$
Formula weight	6074
Space group	$P3_121$
Unit cell dimensions	
a (Å)	62.77
b (Å)	62.77
c (Å)	43.03
No. formula in asymmetric unit	1
Crystal size (mm)	0.3 × 0.3 × 0.1
Resolution (Å)	7.0–3.0
No. reflection measured	21,133
No. unique reflections	1839 (95% complete)
R_{sym}	0.075
No. water molecules	0
R-factor (all data)	0.212
Free-R (10% data)	0.261
RMS deviations from ideal stereochemistry	
Bond distances (Å)	0.012
Bond angles (°)	3.4
Dihedral angles (°)	24.0

Model building of an RNA:DNA hybrid complexed with F8AMD

The initial RNA:DNA–F8AMD complex model was built from the crystal structure of DNA:DNA–F8AMD by modifying the deoxyribose moieties in strand-2 to ribose moieties. The model crystal structure was refined using the method of simulated annealing and following the POSITIONAL refinement with the program X-PLOR.[28] In the calculation, the weight (WA) for the X-ray contribution part that was 65,679.3 for the crystal structure refinement was set to a very small number (1.0) so that the energies of the molecular geometry and interaction were only minimized. Neither water nor counter ions were added in the model. The DNA:DNA–F8AMD model structure was built with a similar procedure used for the RNA:DNA–F8AMD structure, in order to compare the crystal structure. The total energy of the RNA:DNA–F8AMD model system was convergent at −88.3 kcal/mol, whereas the total energy of DNA:DNA–F8AMD model system was 11.4 kcal/mol.

Hairpin stem-loop syntheses

The hairpin stem-loops of 29-mer DNA and RNA–DNA hybrid (Fig. 6), in which the AMD binding site (-GC-) is in the middle of the same sequence, were synthesized at 3 μM scale by a Cruachem PS-250 DNA/RNA synthesizer using the protocol provided from the company. For the RNA–DNA hybrid, the 17-mer DNA was initially synthesized and then the subsequent 12-mer RNA was synthesized. After the deprotection procedure, the crude oligonucleotides were purified by reverse-phase HPLC using a C_{18} column.

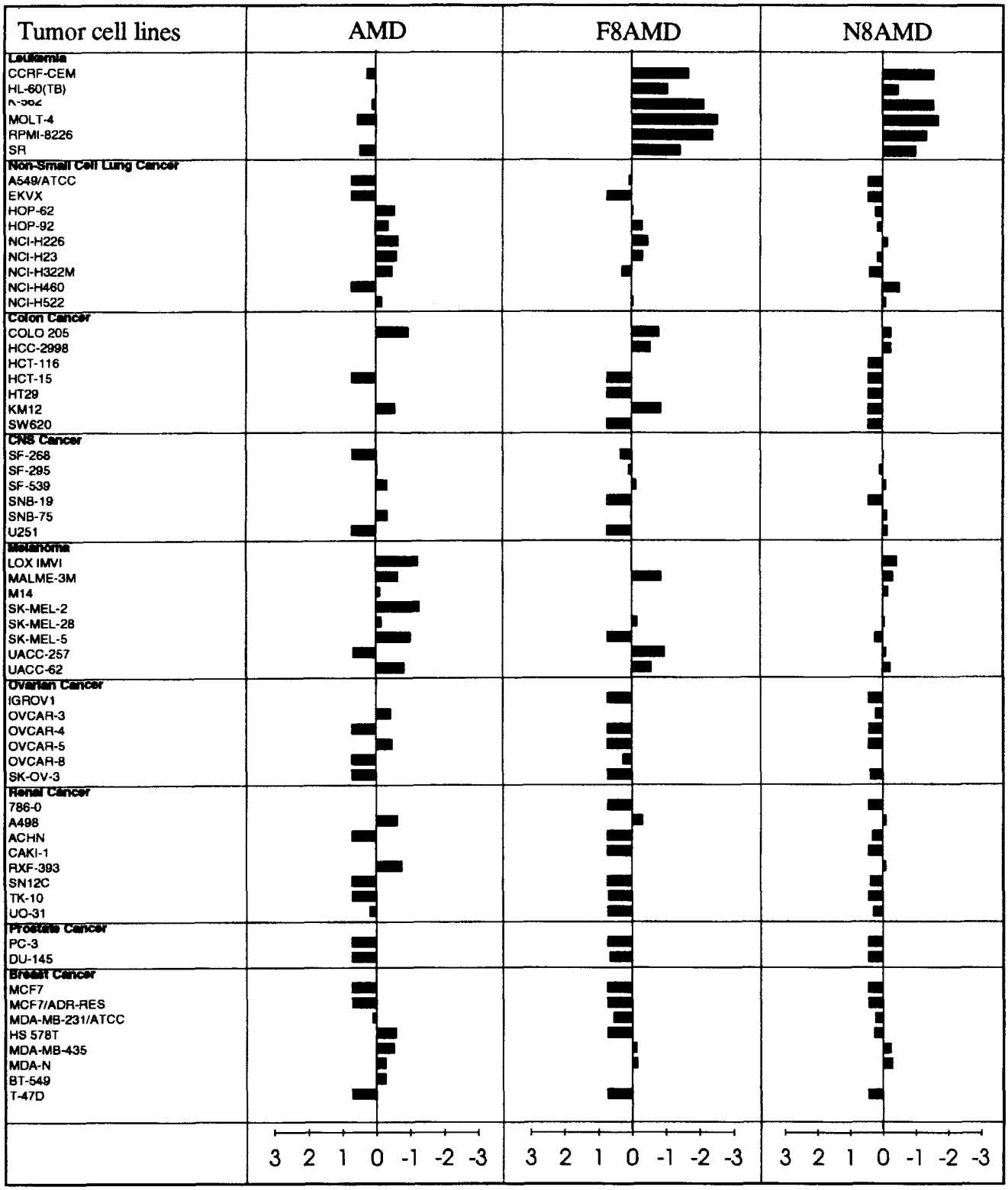

Figure 8. Mean graphs of total growth inhibition (TGI) of AMD, F8AMD, and N8AMD showing the selectivity against various tumor cells. The units of the graphs are $\log_{10}$TGI, and the left and right edges are +3.0 and −3.0, respectively. The mean $\log_{10}$TGI for AMD, F8AMD, and N8AMD are −7.32, −5.72, and −4.56, respectively. For example, the F8AMD data indicate that the leukemia cell growths are totally inhibited at about a 100- to 1000-fold-lower drug concentration than the mean drug concentration required to inhibit the rest of the tumor cells.

UV–vis spectrum measurements

UV–vis absorption spectra were measured on a JASCO V-560 double-beam spectrometer. All measurements were carried out at 1 °C in order to prevent DNA and RNA:DNA melting. The cuvette chamber was slightly modified to fill with −100 °C dew-point dry air to prevent the condensation of moisture on the cuvette

windows. Stock solutions (20 μM) of the DNA and RNA–DNA hairpin stem-loop were prepared with binding buffer (50 mM Tris–HCl pH 7.5, 10 mM $MgCl_2$, and 10 mM KCl). All binding experiments were carried out in the same buffer. The concentrations of the hairpin stem-loops were determined from the absorbance at 260 nm using the extinction coefficients 2.932×10^5 $M^{-1}cm^{-1}$ for the DNA hairpin stem-loop and 2.994×10^5 $M^{-1}cm^{-1}$ for the RNA–DNA hairpin stem-loop.[30] The concentrations of AMD and F8AMD solutions were determined from the absorbances at 440 nm using an extinction coefficient of 2.45×10^4 $M^{-1}cm^{-1}$.[31]

The absorption spectra of drugs during titration with the DNA and RNA–DNA hairpin stem-loops were stored on a computer disk to examine the binding characteristics of drugs to the hairpin stem-loops. After the absorbance of 1.0 mL of drug solution (≈ 1.0 μM) in the binding buffer was measured from 600 to 350 nm at 1 °C, a small aliquot of a known concentration of the DNA solution was placed in the sample cuvette, and spectra were measured 10 min later. This procedure was repeated six times so that six spectra were measured at six different DNA concentrations. The absorbances of visible spectra were read at 1-nm intervals. Dilution factors were applied to all spectra. The base line of the spectrum of F8AMD was slightly corrected with a straight-line addition/subtraction, in order to superimpose the spectrum on the AMD spectrum. The association constants of AMD and F8AMD were calculated based on the spectra using the method developed in our laboratory.[23]

DNA melting measurements

A JASCO HMC-358 constant temperature cell holder connected with a NESLAB RTE-111 bath circulator was used to obtain the melting profiles of the hairpin stem-loops. A 10 μL aliquot of the hairpin stem-loop solution (20 μM) was added into the sample cuvette containing 990 μL of binding buffer, and the absorption at 260 nm was measured from 0 to 65 °C. The cuvette temperature was monitored by putting a thermocouple directly in the cuvette; it increased approximately 0.5 °C/min.

RNA polymerase inhibition

Human (HeLa) cells were cultured at 37 °C in a 1:1 mixture of DME and Harn's F-12 medium, supplemented with penicillin and streptomycin and 5% fetal bovine serum, in an atmosphere of 5.5% CO_2, using a total sodium bicarbonate concentration of 2.3 g/L. The cells were incubated in duplicate cultures with various concentrations of the drugs for 30 min. Then 10 mCi of [^{3}H] uridine were added to label the RNA synthesized during a 30 min incubation at 37 °C. The labeled RNA was isolated by the rapid procedure of Chomczynski and Sacchi.[32] This involves homogenization of the cells in the presence of guanidine thiocyanate to inhibit RNases, acid phenol/chloroform extraction to remove protein and DNA, concentration by isopropanol precipitation, and dissolving the RNA in TE (10 mM Tris–HCl [pH 8.0], 1 mM EDTA). The label incorporated into RNA was determined by liquid scintillation counting.

Anticancer screening test

Anticancer screening tests were carried out at the National Cancer Institute of the National Institutes of Health. The cell panel consists of 60 lines against which compounds are tested at a minimum of five concentrations at 10-fold dilution. A 48-h continuous drug exposure protocol was used, and a sulforhodamine B protein assay was used to estimate cell viability or growth.[33]

Acknowledgements

We wish to thank Mrs Judy Bevan for technical help with the transcription inhibition experiments, Dr Miho Shinomiya for the initial crystallization of the DNA–F8AMD complex, and Dr V. L. Narayanan, Drug Synthesis and Chemistry Branch, National Cancer Institute for the antitumor screening. This research is supported by the NIH (AI28578), Marion Merrell Dow Foundation, J. R. and Inez W. Jay Research Foundation and Kansas Health Foundation, Wichita, Kansas. The Kansas Health Foundation is an independent, nonprofit organization whose mission is to improve the quality of health in Kansas.

References

1. Perun, T. J.; Propst, C. L. In *Nucleic Acid Targeted Drug Design*; Propst, C. L.; Perun, T. J., Eds.; Marcel Dekker: New York, 1992; pp 1–12.

2. Wain-Holson, S.; Sonigo, P.; Danos, O.; Cole, S.; Alizon, M. *Cell* **1985**, *40*, 9.

3. Swanstorm, R.; Varmus, H. E.; Bishop, J. M. *J. Biol. Chem.* **1981**, *256*, 1115.

4. Resnick, R.; Omer, C. A.; Faras, A. J. *J. Virol.* **1984**, *51*, 813.

5. Omer, C. A.; Faras, A. J. *Cell* **1982**, *30*, 797.

6. Gerard, G. F. *Biochemistry* **1981**, *20*, 256.

7. Champoux, J. J.; Gilboa, E.; Baltimore, D. *J. Virol.* **1984**, *49*, 686.

8. Verma, I. M. *Biochim. Biophys. Acta* **1977**, *473*, 1.

9. Müller, W. E. G.; Zahn, R. K.; Seidel, H. J. *Nat. New Biol.* **1971**, *232*, 143.

10. McDonnell, J. P.; Quintrell, N.; Garapin, A.-C.; Fanshier, L.; Levinson, W. E.; Bishop, J. M. *Nature (London)* **1970**, *228*, 433.

11. Kamitori, S.; Takusagawa, F. *J. Mol. Biol.* **1992**, *225*, 445.

12. Kamitori, S.; Takusagawa, F. *J. Am. Chem. Soc.* **1994**, *116*, 4154.

13. Shinomiya, M.; Chu, W.; Carlson, R. G.; Weaver, R. F.; Takusagawa, F. *Biochemistry* **1995**, *34*, 8481.

14. Chu, W.; Kamitori, S.; Shinomiya, M.; Carlson, R. G.; Takusagawa, F. *J. Am. Chem. Soc.* **1994**, *116*, 2243.

15. Filler, R. In *Organofluorine Compounds in Medicinal Chemistry and Biomedical Applications*; Filler, R.; Kobayashi, Y.; Yagupolskii, L. M., Eds.; Elsevier: Amsterdam, 1993; pp 1–22.

16. Sobell, H. M.; Jain, S. C. *J. Mol. Biol.* **1972**, *68*, 21.

17. Meienhofer, J.; Atherton, E. In *Structure–Activity Relationships among the Semisynthetic Antibiotics*; Perlman, D., Ed.; Academic: New York, 1977; pp 427–529.

18. Wang, A. H. J.; Fujii, S.; van Boom, J. H.; van der Marel, G. A.; van Boeckel, S. A. A.; Rich, A. *Nature (London)* **1982**, *299*, 601.

19. Horton, N. C.; Frinzel, B. C. *Am. Cryst. Assoc. Abs.* **1995**, *23*, M099.

20. Dickerson, R. E. *Nucl. Acids Res.* **1989**, *17*, 1797.

21. Dickerson, R. E.; Kopka, M. L.; Pjura, P. *Chemica Scripta* **1986**, *26B*, 139.

22. Müller, W. *Naturwissenschaften* **1972**, *49*, 156.

23. Chu, W.; Shinomiya, M.; Kamitori, K.; Kamitori, S; Carlson, R. G.; Weaver, R. F.; Takusagawa, F. *J. Am. Chem. Soc.* **1994**, *116*, 7971.

24. Dixon, D. A.; Smart, B. E. In *Selective Fluorination in Organic and Bioorganic Chemistry*; Welch, J. T., Ed.; ACS Symposium Series 456, American Chemical Society: Washington, DC, 1991; pp 18–35.

25. Scamrov, A. V.; Beabealashvilli, R. Sh. *FEBS Lett.* **1983**, *164*, 97.

26. Tanaka, I.; Yao, M.; Suzuki, M.; Hikichi, K.; Matsumoto, T.; Kozasa, M.; Katayama, C. *J. Appl. Cryst.* **1990**, *23*, 334.

27. Takusagawa, F. *J. Appl. Cryst.* **1992**, *25*, 26.

28. Brünger, A. T. *X-PLOR 3.1. A System for X-ray Crystallography and NMR*. Yale University: New Haven, 1993.

29. Jones, T. A. *Methods Enzymo.* **1985**, *115*, 157.

30. Cantor, C. R.; Warshaw, M. M. *Biopolymer* **1970**, *9*, 1059.

31. Chen, F.-M. *Biochemistry* **1988**, *27*, 6393.

32. Chomczynski, P.; Sacchi, N. *Anal. Biochem.* **1987**, *162*, 156.

33. Grever, M. R.; Schepartz, S. A.; Chabner, B. A. *Seminars in Oncology* **1992**, *19*, 622.

(*Received in U.S.A.* 22 *August* 1996; *accepted* 18 *February* 1997)